Integral Hot Stamping Process of Tailor-Welded Door Ring Based on the Multi-objective Optimization Genetic Algorithm

Y. L. Song[1,2,3(✉)], J. L. She[1,2], J. Lu[1,2,3], L. Hua[1,2,3], and P. Liu[4]

[1] Hubei Key Laboratory of Advanced Technology for Automotive Components, Wuhan University of Technology, Wuhan 430070, China
ylsong@whut.edu.cn

[2] Hubei Collaborative Innovation Center for Automotive Components Technology, Wuhan University of Technology, Wuhan 430070, China

[3] Hubei Research Center for New Energy and Intelligent Connected Vehicle, Wuhan University of Technology, Wuhan 430070, China

[4] Dongfeng (Wuhan), Industrial Co., Ltd., Wuhan 430070, China

Abstract. To improve the lightweight level of automotive body and solve the internal hot stamping challenges on tailor-welded door ring such as cracking, wrinkling and local distortion, a finite element model of integral hot stamping of a tailor-welded door ring with differential strength and thickness was built. The maximum thinning rate and maximum springback of the door ring were selected as formability indexes, the forming temperature (600–900 °C), coefficient of friction (0.1–0.5) and stamping speed (50–300 mm/s) were taken as variables, and then the response surface method was used to establish the relationship between the process parameter variables and the formability index. Finally, the multi-objective optimization genetic algorithm was used to obtain the optimal combination of process parameters, which provides theoretical guidance for practical production.

Keywords: Door ring · Hot stamping · Formability · Multi-objective Optimization genetic Algorithm · Response surface method

1 Introduction

Auto body component is an important part of automobile, and its high performance and lightweight of manufacturing is an important research direction. The hot stamping process is capable of forming high strength, high stiffness and high precision auto body components. The process is to heat and retain the boron steel blank in a furnace at 900–950 °C, making it completely austenitized, then send it to the die for stamping, and finally the austenite is transformed into martensite by rapid quenching under pressure, resulting in structure strengthening of the formed parts [1].

Hot Stamping Process of High Strength Steel is thermal-mechanical-phase transition coupling process, and the thermal, mechanical properties and microstructure of the

Y. Zhang and M. Ma (Eds.): ICHSU 2022, AHMST 2, pp. 301–310, 2023.
https://doi.org/10.2991/978-94-6463-114-2_42

material are closely related to temperature, so the temperature in the hot stamping process directly affects the quality of the formed parts. Therefore, most of the research on hot stamping has been focused on temperature [2, 3]. With the increased in size and structural complexity of auto body components, single-strength hot stamped parts are no longer able to meet the needs of lightweight and crashworthiness. The application of laser tailor-welded blanks can significantly reduce the vehicle weight and improve the material utilization, and also achieve the forming of parts with different strengths and thicknesses to meet the requirements of the crashworthiness [4].

The door ring is a typical large size and complex structure of the auto body component, which has attracted the attention of many scholars. The design of the door ring determines the final performance distribution of the parts, so the design of the door ring is particularly important. In order to improve the driving safety and reduce the mass of the vehicle, most of the current research on door ring designs have been based on crash simulations, which studied the thickness matching and the seam design [5]. Due to the complexity of door ring forming, simulation studies on door ring forming are very limited, and the object of research is not the door ring with differential strengths differential thicknesses [6]. In addition, some experimental studies have been carried out on defects such as cracking, wrinkling and large springback in door ring forming, but most of the experimental studies were based on process optimization using traditional methods [7, 8]. Therefore, the research on the hot stamping process of tailor-welded door ring is in the initial stage, and some critical challenges still exist in actual production.

In this work, the response surface method combined with genetic algorithm was proposed for multi-objective optimization of door ring forming to improve the formability of door ring.

2 Finite Element Modelling of Integral Hot Stamping of Tailor-Welded Door Ring

2.1 Mechanical Properties the Used of Materials

B1500HS boron steel was used as the experimental material, and the specific heat capacity, thermal expansion coefficient and thermal conductivity are listed in Table 1. Figure 1 shows the true stress-strain curves for 0.1 s^{-1}, 1.0 s^{-1} and 10 s^{-1} at different temperatures from 600 °C to 900 °C. The true stress-strain curves shown in Fig. 1 indicate that the flow stress decreases with increasing temperature and increases with increasing strain rate. Figure 2 shows the forming limit curve of B1500HS at 850 °C [9].

Table 1. Thermo-physical properties parameters [9].

Specific heat [mJ/mm^{3}K]	Thermal expansion [1/K]	Heat conductivity [W/mK]
4.37	1.3×10^{-5}	32

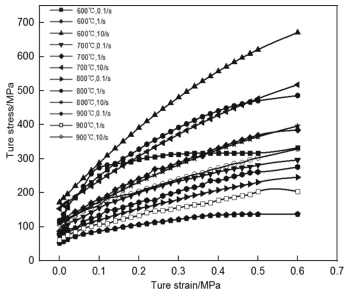

Fig. 1. Flow curves of B1500HS [9].

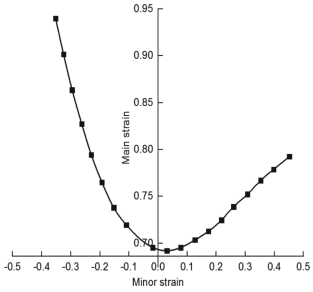

Fig. 2. FLC of B1500HS at 850°C [9].

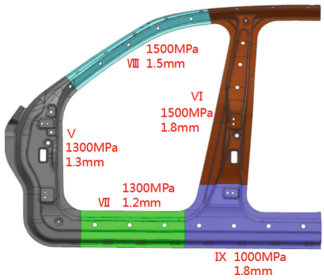

Fig. 3. Three-dimensional diagram of door ring.

2.2 Finite Element Modelling of Door Ring Hot Stamping

Figure 3 shows the three-dimensional part diagram of an automobile door ring designed by UG, which consists of A-pillar, B-pillar, threshold beam and roof side beam, and five weld seams were used to merge each part. Its maximum profile size is 1800 mm × 1400 mm.

The geometric model created by UG has been imported into AutoForm, using AutoForm to define the stamping direction of the door ring, and then to design the process tool face. The finite element model of the drawing process after completing the design of the process addendum surface and binder surface is shown in Fig. 4.

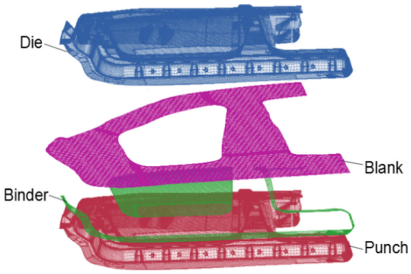

Fig. 4. Finite element model of drawing process.

3 Matching Design of Door Ring Strengths and Dies Temperature

3.1 Matching Design of Door Ring Strengths

Based on the comprehensive consideration of the formability of the door ring, the lightweight of the vehicle and the crashworthiness. The design of the door ring strengths is shown in Fig. 3, as the final tensile strength of hot stamped parts are related to the cooling rate, and local slow cooling can control the cooling rate, thus change the dies temperature has been considered to achieve local slow cooling.

3.2 Matching Design of Dies Temperature

In this work, the relationship between the dies temperature and the tensile strength of the part after forming is determined by the U-shape beam hot stamping simulation. The hot forming simulation was carried out with the forming temperature of 850 °C, the friction coefficient of 0.3 and the stamping speed of 125 mm/s as the process parameters, the dies temperatures set into AutoForm were 150 °C, 200 °C, 250 °C, 300 °C, 350 °C, 400 °C, 450 °C, 500 °C and 550 °C respectively [10]. The tensile strength of the part was obtained as shown in Fig. 5. According to the influence of dies temperature on the tensile strength of part, the dies temperatures at the positions of A-pillar, B-pillar, threshold beam, lower end of B-pillar and roof side beam have been set to 300 °C, 200 °C, 300 °C, 550 °C and 200 °C respectively, the dies temperature design is shown in Fig. 6.

3.3 Preliminary Hot Stamping Simulation Results of Door Ring

With the forming temperature of 850 °C, the friction coefficient of 0.3 and the stamping speed of 125 mm/s as process parameters for the preliminary forming simulation of the door ring, the preliminary simulation results were obtained as shown in Fig. 7(a) and Fig. 7(b), with a maximum thinning rate of 32.7% and a maximum springback of 7.768 mm after trimming. However, the thinning rate and the springback after trimming directly affect the forming quality and accuracy of the final part. Therefore, it is necessary to optimize the maximum thinning rate and the maximum springback after trimming.

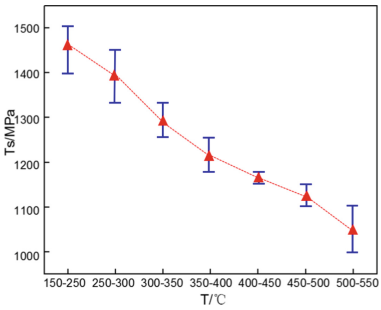

Fig. 5. Tensile strength of the door ring at different dies temperatures.

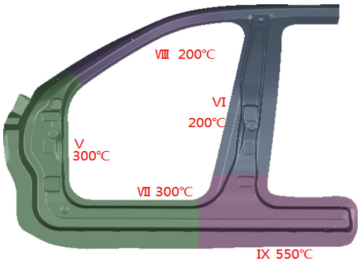

Fig. 6. Design of dies temperatures.

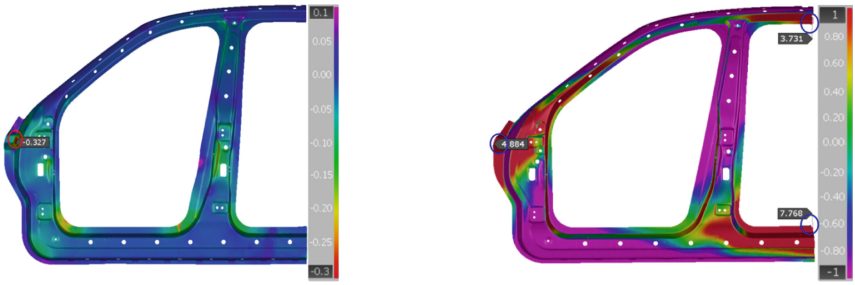

Fig. 7. (a) Thinning rate distribution of door ring, (b) Springback distribution of door ring.

4 Multi-objective Optimization of Door Ring Hot Stamping Process

As the different process parameters have different effects on the forming law, in order to improve the forming properties and control the springback, the second-order response surface model between the process parameters and the target was established using the CCD (central composite design), and combined with the NSGA-II algorithm for multi-objective optimization.

4.1 Response Surface Modelling and Analysis of Variance

Design-Expert software was used to select 3 factors and 5 levels for the CCD, T (the forming temperature), μ (the friction coefficient between the dies and the blank) and v (the stamping speed) were used as the variables for the process parameters, and the maximum thinning rate in the drawing process and the maximum springback after the trimming process were used as the objective response Y. The combinations of 27 different factors were obtained, and these different combinations have been input and calculated in AutoForm. The data on the maximum thinning rate of the drawing and the maximum springback after trimming obtained according to the designs are shown in Table 2.

Based on the test design point data, the second-response model for the objective function of thinning rate D_f and the objective function of springback D_{spr} were obtained, as shown in Eq. (1) and Eq. (2).

$$D_f = 28.88 + 0.62T + 8.27\mu - 3.68v - 0.025\mu - 0.28Tv - 0.37v\mu + 0.49T^2 + 4.49\mu^2 + 2.89v^2 \quad (1)$$

$$D_{spr} = 5.03 - 0.71T - 0.32\mu + 0.011v + 0.22T\mu + 5.875 \times 10^{-3}Tv - 0.043v\mu + 0.45T^2 + 2.39\mu^2 - 2.03v^2 \quad (2)$$

The second-order response surface models for the maximum thinning rate and maximum springback were calculated from the data in Table 2, and the F-values of the two models were 50.29 and 32.03 respectively, and the P-values were less than 0.0001, indicating that the effect of the models on the maximum thinning rate and maximum springback was very significant and credible.

Figure 8(a) and Fig. 8(b) show the interaction of the forming temperature and the friction coefficient on the maximum thinning rate and the maximum springback respectively. It could be seen that when the stamping speed was constant, the maximum thinning

Table 2. Design matrix and simulation results of the experiment.

No.	Temperature [°C]	Friction coefficient	Stamping speed [mm/s]	Thinning rate [%]	Springback [mm]
1	825	0.3	175	30.9	4.956
2	825	0.3	175	30.9	4.956
3	750	0.3	237.5	26.9	4.617
4	750	0.3	112.5	32.7	5.014
5	750	0.3	175	28.7	4.825
6	750	0.3	175	28.7	4.825
⋮	⋮	⋮	⋮	⋮	⋮
26	900	0.1	50	32.7	5.509
27	900	0.1	300	25.3	4.722

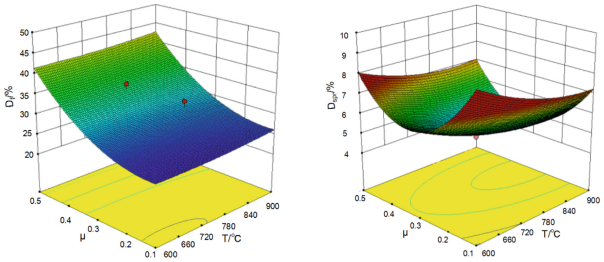

Fig. 8. (a) Response surface of the maximum thinning rate, (b) Response surface of the maximum springback.

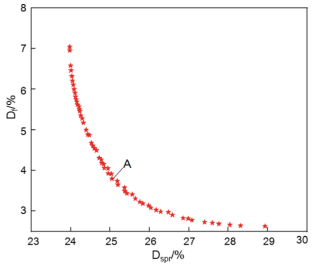

Fig. 9. Effect of process parameter solution set on springback and thinning rate.

rate and the maximum springback tended to increase approximately with the increased in forming temperature and the friction coefficient, but the influence on the maximum springback is complex. In order to ensure that the thinning rate of the drawing process reaches the production requirements and the springback after trimming is as small as possible, it is necessary to use the multi-objective optimization to obtain a suitable combination of process parameters.

4.2 Multi-objective Genetic Algorithm

NSGA-II is an improved multi-objective optimization algorithm of the NSGA (Non-Dominated Sorting Genetic Algorithm), which is widely applied in the multi-objective optimization of process parameters. In order to ensure that the maximum thinning rate after drawing meets the part thickness requirements, and that the maximum springback after trimming is as small as possible, the objective function and constraints for multi-objective optimization were established as follows:

$$F = \min[D_f(\%), D_{spr}(mm)]$$
$$\begin{cases} 600 \leq T \leq 900°\text{C} \\ 0.1 \leq \mu \leq 0.5 \\ 50 \leq v \leq 300\,\text{mm/s} \end{cases} \tag{3}$$

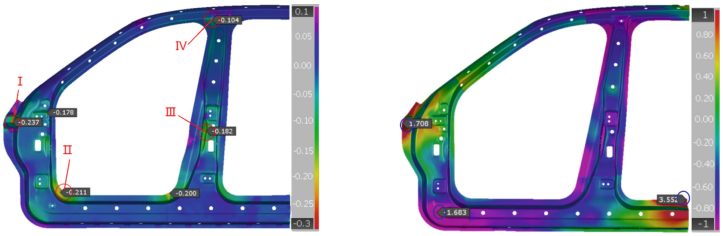

Fig. 10. (a) Thinning rate distribution of door ring, (b) Springback distribution of door ring.

By the multi-objective optimization algorithm, the Pareto optimization solution of the objective function space was obtained and is shown in Fig. 9. Each point in Fig. 6 represents a non-inferior optimal stamping process parameter solution obtained by the optimization.

5 Optimized Simulation Verification of Tailor-Welded Door Ring

5.1 Simulation Verification

From Fig. 9, taking the maximum thinning rate $D_f \leq 25\%$ and the maximum springback D_{spr} to be the smallest possible as the ultimate optimization objective. Therefore, point A in Fig. 7 was chosen for the verification. The combination of process parameters of point A ($T = 875$ °C, $\mu = 0.146$, $v = 195$ mm/s) was input into AutoForm for the verification. Some of the optimization results are shown in Fig. 10, Fig. 10(a) shows that under the combination of process parameters at point A, the larger thinning rate appears in I, II, III and IV areas, and the maximum thinning rate is 23.7% ($D_f \leq 25\%$). Figure 10(b) shows that the maximum springback after trimming is 3.552 mm, it can provide reference for springback compensation. The simulation value is close to the optimized prediction value, and the forming quality is good.

5.2 Structure Analysis

Figure 11 show the martensite distribution of the part obtained by simulating with the process parameters at point A. Figure 11 indicates that the martensite transformation in the V, VI, VII and VIII areas was full, while in the IX area the martensite transformation rate was mostly between 70 and 80%. Figure 12 show the tensile strength and design tensile strength distribution of the part obtained by simulating with the process parameters at point A. As can be seen from Fig. 12, the average tensile strength was close to design tensile strength.

Although the transformation of martensite in V and VII areas is full, but the cooling rate is lower when the martensitic phase transformation occurs compared to VI and VII areas, so the martensite structure is thicker, and the tensile strength is lower. The proportion of martensite in the IX area is low and the bainite is relatively high. Because of the martensite is hard phase, so the lower the martensite component, the smaller tensile strength and the better crashworthiness [11].

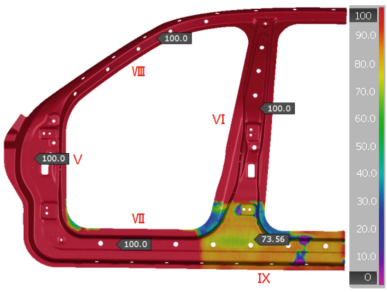

Fig. 11. Martensite distribution of door ring.

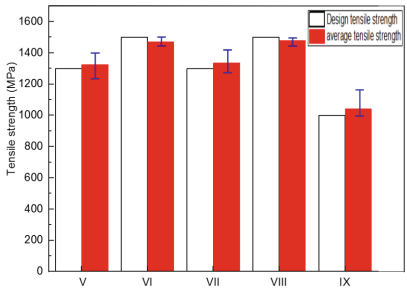

Fig. 12. Tensile strength distribution of door ring.

6 Conclusion

Aiming at the integral hot stamping of door ring with differential strengths and thicknesses, the matching design of dies temperature was carried out and the partial cooling scheme was determined to achieve partial softening. The central composite design and genetic algorithms to achieve multi-objective optimization was adopted to change process parameters.

Simulation results show that the prediction values were close to the target value ($D_f = 23.7\% < 25.0\%$ and $D_{spr} = 3.552$ mm). The local tensile strengths, thinning rate and springback of the door ring meet the design requirements.

Acknowledgments. This work was financially supported by National Natural Science Foundation of China (Grant No. 51975440), the 111 Project (Grant No. B17034), the Fundamental Research Funds for the Central Universities (WUT: 2022III006XZ) and the Innovative Research Team Development Program of Ministry of Education of China (Grant No. IRT17R83).

References

1. M. Merklein and J. Lechler, Investigation of the thermo-mechanical properties of hot stamping steels, *J. Mater. Process.* **177**, 452 (2007).
2. K. Mori, S. Maki and Y. Tanaka, Warm and hot stamping of ultra high tensile strength steel sheets using resistance heating, *CIRP Ann. Manuf. Technol.* **54**, 209 (2005).

3. J. Lu, Y. L. Song, L. Hua, J. N. Liu and Y. H. Shen, Influence of thermal deformation conditions on the microstructure and mechanical properties of boron steel, *Mater. Sci. Eng. A* **701**, 328 (2017).
4. R. Kolleck, R. Vollmer, C Both and A Breuer, Investigation of weld seam structures of tailor welded blanks for hot stamping, *Key Eng. Mater.* **3910**, 639 (2015).
5. E. Altınok, H. Kayserili, A. Mert and S. A. Altınel, Lightweight door ring solution in car body development, *Adv. Auto. Technol.* **1**, 131 (2017).
6. D. Qing, W. Shen and Z. J. Wang, Optimization design of hot stamping integrated door knocker based on CAE analysis technology, *Chinese VW.* **22**, 56 (2020).
7. J. Yang, X. F. Qin and Z. W. Li, Manufacturing process for hot forming door rings, *Chinese Forging & Stamping Technol.* **46**, 71 (2021).
8. Z. G. Yan, C. M. Shen, Hot stamping integral door ring forming die and process development, *Chinese Automobile and New Powertrain* **4**, 75 (2021).
9. R. Z. Liu, Y. L. Song and P. Liu, Multi-objective optimization design of strength distribution of automotive central pillar based on Gray-Taguchi method, *Chinese J. Plast. Eng.* **28**, 29 (2021)
10. Y. Chen, Z. Q. Sun and X. X. Zhang, Influence of die temperature and bonding state for hot stamping on microstructure and properties of 22MnB5, *Chinese J. Plast. Eng.* **28**, 11 (2021).
11. Q.G. He, Development and research of 1500MPa hot formed high strength steel containing vanadium, Master thesis, Northeastern University (2018).